Characterization of supported platinum nanoparticles by ^{195}Pt solid-state NMR

Spectroscopic background: ^{195}Pt nuclei have a spin of I = 1/2 and, therefore, no quadrupole moment. The ^{195}Pt isotope has a natural abundance of 33.8 %, a resonance frequency of ν_0 = 107.51 MHz at B_0 = 11.75 T, and a sensitivity of 3.5 x 10^{-3} in comparison with ^{1}H nuclei (1.0). For basic principles of solid-state NMR, see lectures “Solid-State NMR Spectroscopy” for Bachelor students or PhD seminars, accessible via the link “Lectures for Students”.

Platinum is an important catalytically active component for hydrogenation [1], dehydrogenation [2], hydrocracking [3], hydroisomerization [4], hydrodeoxygenation [5], and hydrogenolyse reactions [6, 7], as well as fuel cells [8], and for PHIP NMR experiments [9]. Because of the high sensitivity of ^{195}Pt solid-state NMR spectroscopy for the nature and properties of platinum atoms, this method is broadly applied for the characterization of platinum nanoparticles deposited on carbon black [8, 24], TiO_2 [11, 16, 17], alumina [11, 12, 14], silica [11, 13], and zeolitic [15, 18] supports. ^{195}Pt solid-state NMR spectra of platinum nanoparticles can be best explained by a **layer model**. This model yields a relationship between the sizes of nanoparticles and the number of atoms in each layer of the particles (**Fig. 1**) [8].

layers of a platinum nanoparticle

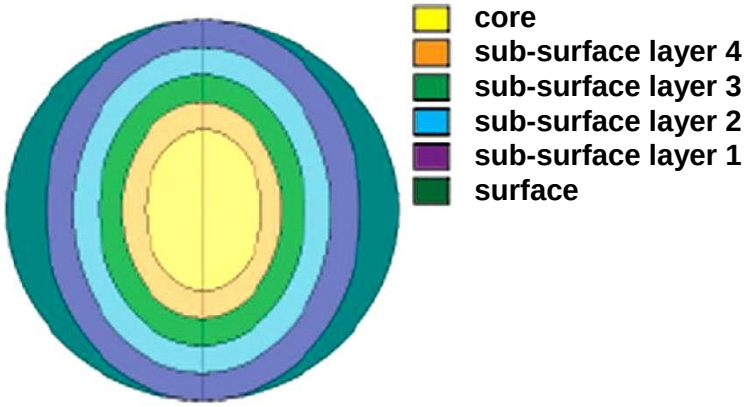

Fig. 1

The position and shape of ^{195}Pt solid-state NMR signals of platinum atoms in nanoparticles are influenced by several contributions. In contrast to the smallest platinum cluster, Pt_{13}, which is characterized by anomalous diamagnetic properties [21], ^{195}Pt atoms in the various layers **of platinum nanoparticles with larger size**

are affected by Knight shift interactions and their different local symmetries may lead to significant linewidths. Therefore, platinum atoms in each of the various layers in the model in **Fig. 1** represent a distinct ^{195}Pt solid-state NMR spectrum.

The inner layers of a platinum nanoparticle have a metallic character and contain conduction electrons. The spins of these conduction electrons are polarized by the external magnetic field giving rise to a Knight shift of resonating ^{195}Pt nuclei. Usually, Knight shifts are much greater in magnitude than the diamagnetic shielding. The total resonance shift of ^{195}Pt atoms in platinum nanoparticle is given by [8]:

$$\text{total shift} = \sigma + K_s + K_d^{orb} + K_{cp} \quad (1)$$

where σ is the diamagnetic shielding, K_s represents the s-electron contribution to the Knight shift, and K_d^{orb} describes the d-electron involvement. The contributions of K_s and K_d^{orb} are both positive Knight shifts of ^{195}Pt solid-state NMR signals. If the hyperfine fields of the conduction electrons induce a polarization in the inner core s-electrons, an additional Knight shift can be produced, which is termed core polarization K_{cp}. This polarization term gives a **negative resonance shift of the ^{195}Pt solid-state NMR signal**, as occurring for platinum atoms in the inner metallic cores of nanoparticles [8].

Because of the different experimental techniques (*vide infra*) applied for ^{195}Pt solid-state NMR studies of platinum nanoparticles, specific scales for assigning resonance positions are utilized. In numerous studies, the resonance positions are described by a G/kHz scale (or kG/MHz) [10-14]. In this scale, the resonance position for **"zero Knight shift"** has a value of $\boldsymbol{H_0/\nu_0}$ **= 1.100 G/kHz** [11, 13], which corresponds to the resonance position of H_0 = 81.2 kG at ν_0 = 73.765 MHz (81.200 x 10^3 G / 73.765 x 10^3 kHz = 1.101 G/kHz) in Ref. [12]. The same value, i.e. H_0/ν_0 = 1.100 G/kHz, is attributed to the resonance position of ^{195}Pt atoms **in clean surface layers ("surface peak")** of platinum nanoparticles [10]. The resonance position of ^{195}Pt atoms in the core layers of platinum nanoparticles **("infinite" solid), i.e. in the metallic bulk phase** containing conduction electrons, is $\boldsymbol{H_0/\nu_0}$ **= 1.138 G/kHz** [11, 13]. In numerous studies, the metallic character of these platinum atoms was evidenced by measuring the spin-lattice relaxation time T_1 as a function of temperature T and by correlating $1/T_1$ with T for demonstrating their linear relationship (see, e.g., Fig. 4 in Ref. [11]).

This experimental test for the metallic character and the presence of conduction electrons bases on the Korringa equation [12, 28].

In Ref. [8], the resonance position of platinum atoms in the metallic bulk phase corresponds to a high-field shift value of δ_{195Pt} = -35,350 ppm in a magnetic field of B_0 = 7.05 T. A further scale for describing the Knight shift of ^{195}Pt solid-state NMR signals of platinum atoms in nanoparticles is based on K values given in "%" [11]. For ^{195}Pt atoms in the metallic bulk phase of nanoparticles, Ref. [11] gives a value of K = -3.45 %. Calculating the Knight shift-induced frequency change $\Delta\nu$ via [8]:

$$\Delta\nu = (\gamma_{195Pt} \cdot B_0 \cdot K) / 2\pi \qquad (2)$$

with γ_{195Pt} = 5.84 x 10^7 $s^{-1}T^{-1}$, B_0 = 7.05 T, and K = -3.45 %, a $\Delta\nu$ value of -2.26 MHz is obtained. With the resonance frequency ν_0 = 64.1 MHz of ^{195}Pt nuclei at B_0 = 7.05 T, the above-mentioned $\Delta\nu$ = -2.26 MHz corresponds to a Knight shift of δ_{195Pt} = -35,257 ppm, which agrees well with the shift of δ_{195Pt} = -35,350 ppm in Ref. [8]. In **Table 1**, a survey on the resonance positions of ^{195}Pt atoms in clean surface layers and in the metal bulk phase of platinum nanoparticles for the different scales is given.

Platinum species	H_0 **in kG**	H_0/ν_0 **in *G*/kHz**	K **in %**	δ_{195Pt} **in ppm**
Na_2PtCl_6, 1.2 M in D_2O				0 [8]
clean surface Pt on platinum nanoparticles ("surface peak", "zero Knight shift")	0 [12]	1.100 [13]	0 [12]	
Pt_{13}, diamagnetic clusters				-7,400 [8]
bulk Pt in platinum nanoparticles ("infinite" solid, metallic bulk phase)	84 [12]	1.138 [13]	-3.44 to -3,45 [11]	-35.350 [8]

Table 1

The ^{195}Pt NMR signals of compounds, which are not involved in Knight shift interactions, occur at the low-field side of the "zero Knight shift" (H_0/ν_0 < 1.10 G/kHz), as illustrated in **Fig. 2** [14].

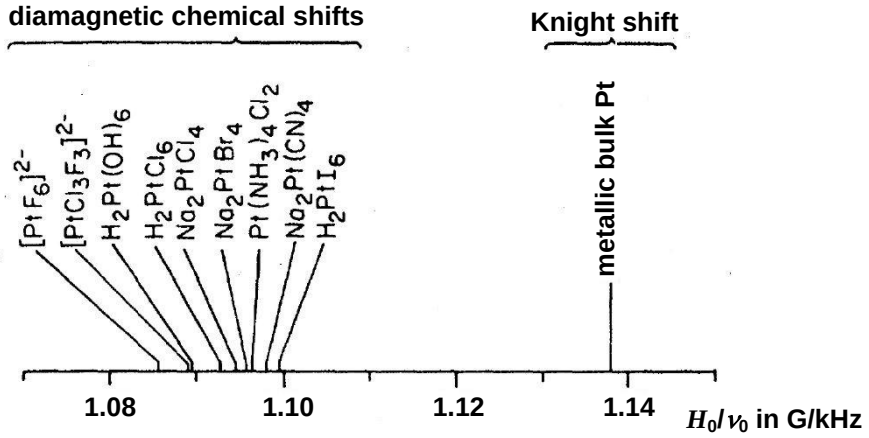

Fig. 2

Because of the large frequency range of solid-state NMR signals of ^{195}Pt atoms in platinum nanoparticles of ca. 3 MHz, single pulse excitation of the whole spectral range is not possible. Therefore, in most of the ^{195}Pt solid-state NMR studies, an **add-subtract $\pi/2-\tau-\pi-\tau$ spin echo experiment** was utilized (see **Fig. 3**) [14]. Inverting the $\pi/2$ pulse inverts the spin echo. By subtraction of the inverted spin echo from the non-inverted one, the spin echoes are effectively added, but the coherent noise due to the π pulse is subtracted out. This experiment is repeated with **step-wise variation of the H_0 field** [12, 14] **or of the resonance frequency** ν_0 [11, 13]. The resulting point-by-point recorded spin echoes deliver data over the broad frequency range of 3 MHz.

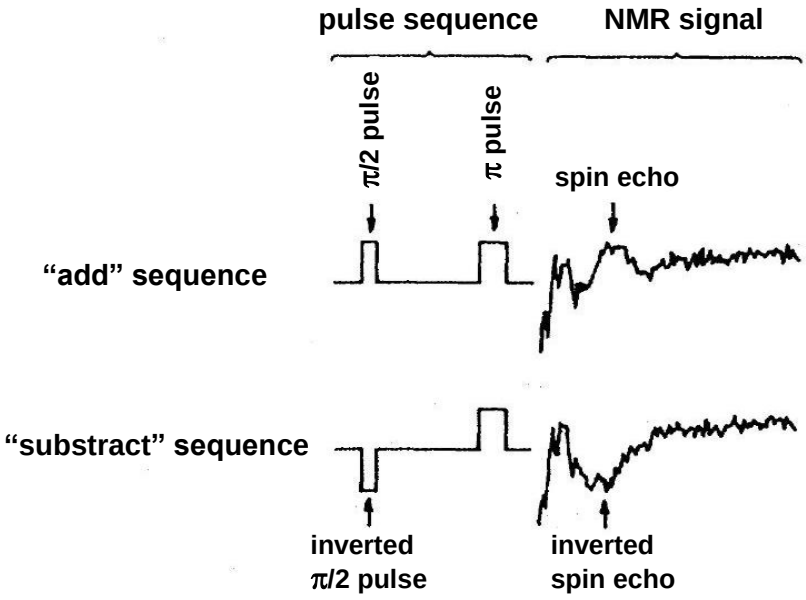

Fig. 3

The point-by-point spin echoes reconstruct the ^{195}Pt solid-state NMR spectra of platinum nanoparticles, which is an often utilized technique throughout the literature [11-14]. Depending on the method for evaluating the spin echoes, these techniques are known as **spin echo height spectroscopy (SEHS)** or **spin echo integration spectroscopy (SEIS)** [8]. Disadvantages of the point-by-point techniques are difficulties with the limited number of sampling points, normalization of the probe tuning, and duration of the NMR experiments. Another conventional method that most of circumvents these limitations is the **variable offset cumulative frequency stepping (VOCS)** technique [8, 19]. The most sophisticated technique is the **field sweep Fourier transform (FSFT)** method that allows an accurate reconstruction of the ^{195}Pt wide-line NMR spectrum with an improved resolution as well as full automation [8]. The field sweep works by tuning to a single upfield frequency and utilizing an additional coil within the main superconducting magnet to shift the B_0 field by B_{sw} = ±0.5 T and sweep through the whole resonance [8, 20].

As an example, **Fig. 4a** shows the ^{195}Pt FSFT NMR spectrum of **platinum nanoparticles with a mean diameter of Ø = 4.8 nm** and a calculated total number of 3871 platinum atoms, which are supported on carbon black [8]. For nanoparticles of this size, 8 distinct layers are predicted, but the three innermost core layers are considered inseparable.

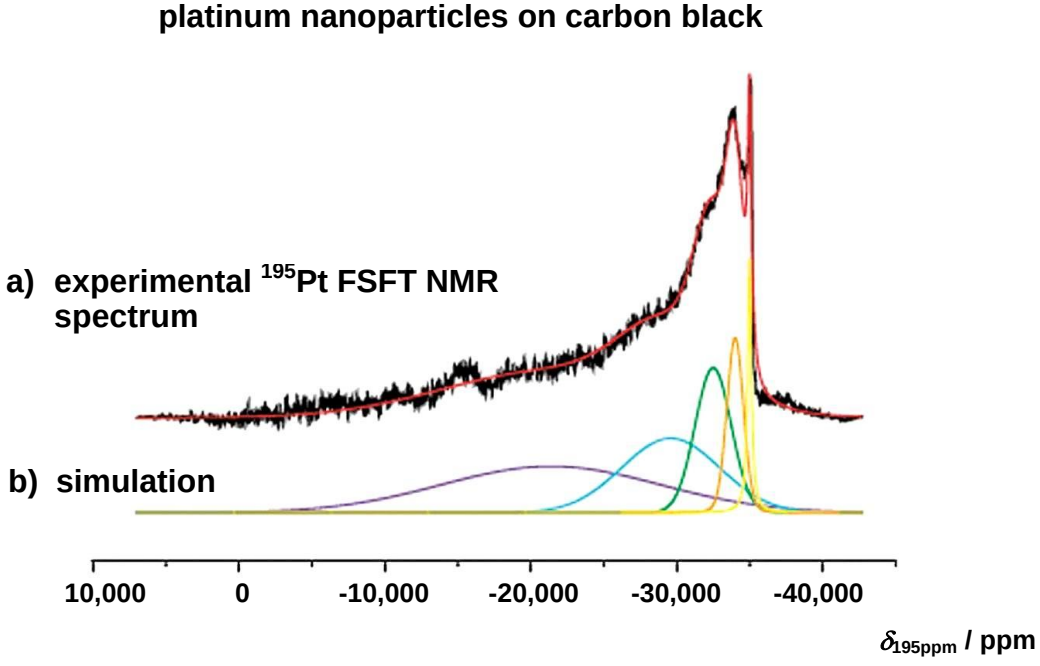

Fig. 4

Fig. 4b depicts the deconvoluted ^{195}Pt FSFT NMR spectrum of the platinum nanoparticles supported on carbon black, assuming five distinct layers with the innermost layers being combined to form a core. The colours of the curves agree with those of the layers in **Fig. 1**. If moving downfield, a decrease of the negative Knight shift and a broadening of the resonances occur. This effect is caused by the platinum atom positions in the different layers from the core to the surface, which are characterized by a loss of the metallic character and an increasing perturbation of their local structures, i.e. a loss of local symmetry of the platinum atoms [8].

The influence of the size Ø of platinum nanoparticles on the shapes of ^{195}Pt SEHS NMR spectra is illustrated in **Fig. 5** [12]. It is obvious that the shapes strongly depend on the **nanoparticle sizes in the range of Ø = 9 to 39 Å** from top to bottom. For the small nanoparticle size of Ø = 9 Å, the echo intensity near the metal peak ($H_0/\nu_0 \cong$ 1.14 G/kHz) is weak, and the echo intensity in the low field region near the surface peak ($H_0/\nu_0 \cong$ 1.09 G/kHz) is large. Contrary, in the ^{195}Pt SEHS NMR spectrum of

^{195}Pt SEHS NMR of platinum nanoparticles on Al_2O_3

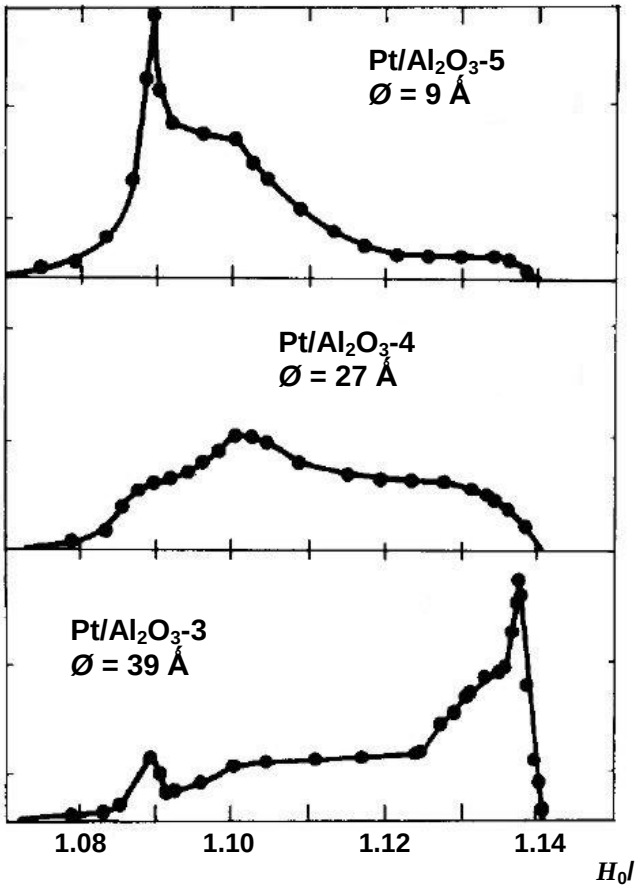

Fig. 5

the large platinum nanoparticles with the size of Ø = 39 Å, the metal peak ($H_0/\nu_0 \cong$ 1.14 kG/MHz) is strong, while the echo intensity at the surface peak ($H_0/\nu_0 \cong$ 1.09 kG/MHz) is weak. By evaluating the intensity distributions in the high field (metallic core platinum) and the low field region (surface platinum), and assuming that the platinum nanoparticles particles are Wulff crystals (cubo-octahedron) [22], the platinum dispersions in column 2 of **Table 1** were calculated for a series of samples with different nanoparticles sizes [14]. These **NMR dispersion values agree reasonably** well with those determined by **hydrogen chemisorption** (column 3) and **electron microscopy** {column 4) [14].

Materials	**Dispersion by ^{195}Pt SEHS NMR in %**	**Dispersion by H_2 chemisorption in %**	**Dispersion by microscopy in %**
Pt/Al_2O_3-1	5	4	
Pt/Al_2O_3-2	8	11	
Pt/Al_2O_3-3	10	15	16
Pt/Al_2O_3-4	19	26	22
Pt/Al_2O_3-5	40	46	61
Pt/Al_2O_3-6	79	58	

Table 1

The sensitivity of ^{195}Pt solid-state NMR spectroscopy for the **treatment conditions of supported platinum nanoparticles** is demonstrated in **Fig. 6** [11]. These spectra were recorded after reduction of platinum supported on TiO_2 with gaseous H_2 at temperatures of T_{H2} = 473 K (open triangles) and T_{H2} = 773 K (open circles). The reduction at T_{H2} = 773 K has a tremendous effect on the line shapes in comparison with that performed at T_{H2} = 473 K. The surface peak at $H_0/\nu_0 \cong$ 1.10 G/kHz does not shift appreciably, but increases in amplitude at the expense of the bulk peak at $H_0/\nu_0 \cong$ 1.14 G/kHz, in comparison with the spectrum recorded after reduction with H_2 at T_{H2} = 473 K. This observation indicates that after reduction at the higher temperature, fewer ^{195}Pt atoms are in inner core layers. A possible explanation is an increasing **strong metal-support interaction (SMSI)** effect upon reduction at the higher temperature of T_{H2} = 773 K [11]. The SMSI phenomenon is a sintering or massive encapsulation of platinum particles by the support material, such as by TiO_2 [23].

^{195}Pt SEHS NMR of platinum nanoparticles on TiO_2

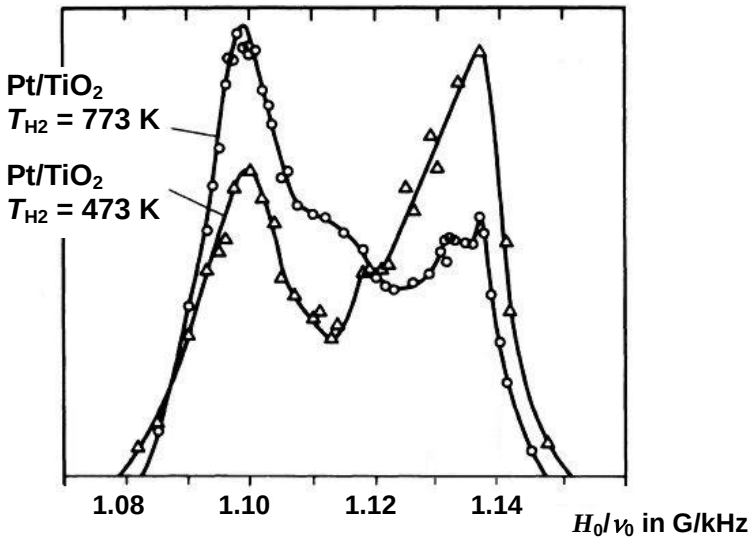

Fig. 6

Another influence on the resonance position and shape of ^{195}Pt solid-state NMR signals of supported platinum nanoparticles is caused by **adsorption of molecules**, such as H_2 [10, 12, 13, 15, 16, 18], O_2 [10, 17, 18, 25], and CO [24, 25, 33], or by thiol-capping [26]. As an example, **Fig. 7** shows ^{195}Pt SEHS NMR spectra of Pt/Al_2O_3-5 (see **Table 1, line 6**) recorded before (top) and after chemisorption of H_2 (bottom) [12]. After exposing hydrogen on the clean platinum nanoparticles, a significant

^{195}Pt SEHS NMR of platinum nanoparticles on Al_2O_3

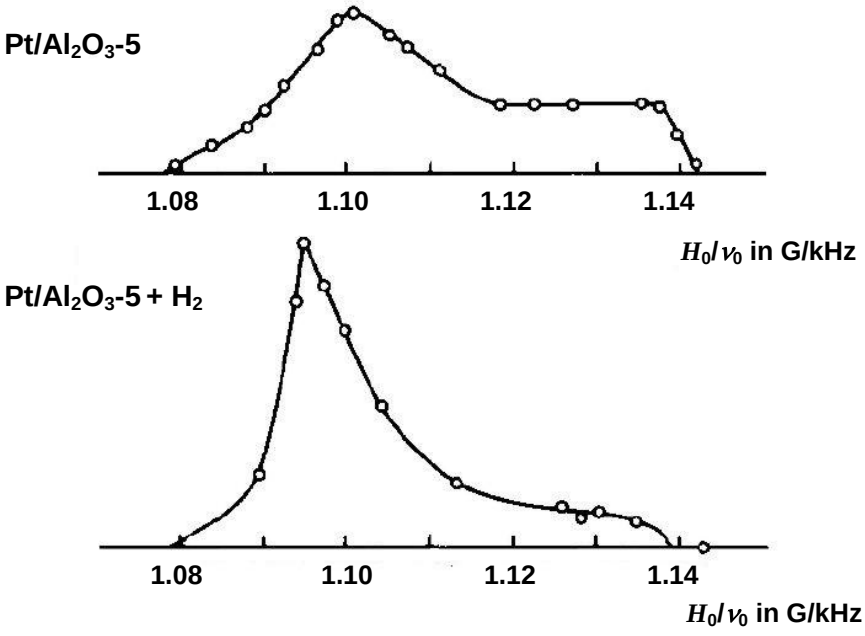

Fig. 7

change of the echo intensity distribution is obvious. The resonance position of the high-field plateau due to metallic bulk platinum atoms occurs at the same position as in the untreated sample, but is significantly decreased. The low-field surface peak shows an intensity increase and another position as well as smaller width. Interestingly, a **shift of the surface peak** from H_0/ν_0 = 1.100 G/kHz to H_0/ν_0 = 1.095 G/kHz occurred. A hydrogen-induced change of the nanoparticle size as a reason for the changed ^{195}Pt SEHS NMR intensity distribution could be excluded by electron microscopy [12]. Therefore, the above-mentioned observations hint at an incorporation of hydrogen atoms into deeper sub-surface layers of the nanoparticles, which leads to a loss of platinum atoms with metallic character.

In Ref. [33], the interaction of CO with platinum nanoparticles on **Pt/Al_2O_3** samples was studied upon **adsorption of ^{13}C-enriched carbon monoxide**. Furthermore, the results of ^{195}Pt SEHS NMR investigations were compared with those of ^{195}Pt SEDOR NMR studies. Originally, **spin echo double resonance (SEDOR)** experiments are utilized for the determination of heteronuclear atom-atom distances, such as of ^{27}Al and ^{31}P atoms in aluminophosphate molecular sieves [34]. In Ref. [33], the SEDOR technique was used for the identification of platinum atoms in the direct vicinity of ^{13}C atoms, i.e. of platinum atoms, which are involved in ^{13}C-^{195}Pt spin couplings. For this purpose, the SEDOR experiment was performed with a spin echo for the ^{195}Pt nuclei, like shown in **Fig. 3**, while an additional π pulse was irradiated in the channel of the ^{13}C nuclei, applied at the same time like the π pulse for the ^{195}Pt nuclei. As in the SEHS experiments, the "add-subtract" technique was utilized for the SEDOR experiments to avoid the interference of "coherent noise" [33].

Fig. 8 shows the ^{195}Pt SEHS NMR and ^{195}Pt SEDOR NMR spectra of platinum nanoparticles supported with a dispersion of 26% on Al_2O_3 (Pt/Al_2O_3) and covered with ^{13}CO [33]. Comparison of the ^{195}Pt SEHS NMR and the ^{195}Pt SEDOR NMR spectra indicates that the former one is very similar to the spectrum of clean Pt/Al_2O_3-5 in **Fig. 7, top**, while the latter one consists exclusively by a peak at H_0/ν_0 = 1.095 G/kHz, which is characteristic for diamagnetic surface platinum atoms bound to adsorbate species. The ^{13}C-^{195}Pt spin couplings, responsible for the low-field peak in **Fig. 8,** lead to a spectrum, which is very similar to those found for diamagnetic platinum carbonyl molecules, such as $[(Pt)_3(CO_6)]^{2-}$, $[(Pt)_6(CO)_{12}]^{2-}$, and $[(Pt)9(CO)18]^{2-}$ [35]. This result evidences that adsorption of ^{13}CO causes the

formation of Pt-C bonds in the surface layers of platinum nanoparticles of Pt/Al_2O_3, which agrees with studies of large single crystals [33].

^{195}Pt solid-state NMR of platinum nanoparticles on Al_2O_3

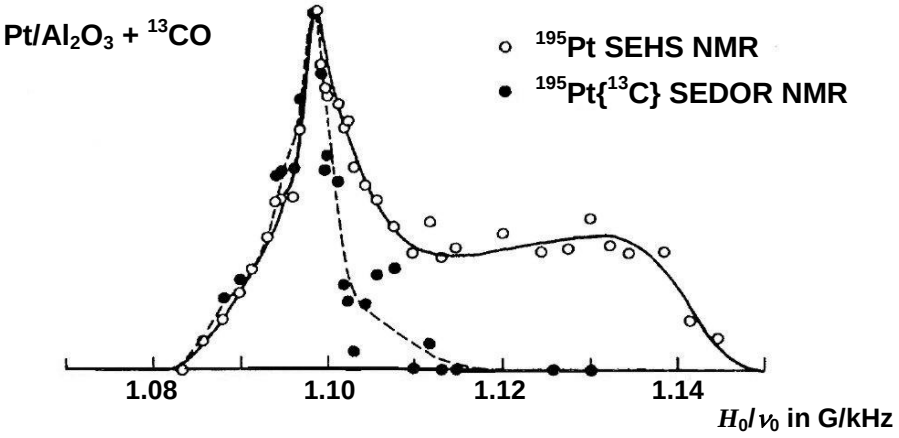

Fig. 8

In Ref. [25], effects of the adsorbate electronegativity on the Knight shifts of platinum atoms in nanoparticles of electrocatalysts were investigated. For a review on NMR techniques for noble metal nanoparticle characterization, including supported platinum nanoparticles, see Ref. [27].

Catalyst preparation: The platinum nanoparticles used for recording the spectrum in **Fig. 4** were synthesized according to Ref. [30], while the Pt_{13} clusters were prepared according to Ref. [31]. The Pt/Al_2O_3 samples used in Ref. [12] for obtaining the spectra in **Figs. 5 and 7** were prepared by impregnation of alumina with a solution of H_2PtCl_6. The resulting material was dried and subsequently calcined and reduced under hydrogen, both at T = 573 K. The durations of these treatments are given in Table 2 of Ref. [12]. The Pt/TiO_2 samples used for the spectra in **Fig. 6** were prepared according to Refs. [11] and [31] by impregnation of TiO_2-anatase (180 m^2/g, Bayer) with an aqueous solution of hexachloroplatinate and subsequent reduction under hydrogen at T = 673 K.

^{195}Pt solid-state NMR studies: The ^{195}Pt FSFT NMR spectrum in **Fig. 4** was recorded at a Larmor frequency of ν_0 = 64.1 MHz and utilizing a B_0 = 7.05 T Magnex

magnet with a B_{sw} = ±0.5 T sweep coil within the main cryostat [8]. For each field sweep study a $\pi/2-\tau-\pi-\tau$ spin echo was adopted, which employed $\pi/2$ and π pulses of 5 µs and 10 µs, respectively, and an echo delay of τ = 20 ms. Each measurement consisted of 50 kHz effective-width slices spanning a frequency range of ν_0 = 61.1 to 64.3 MHz [8]. The ^{195}Pt SEHS NMR spectra in **Figs. 5 and 7** were obtained using a pulse NMR spectrometer, operating at a Larmor frequency of ν_0 = 74 MHz, and at a temperature of T = 77 K [12, 14]. The pulse delays of the $\pi/2-\tau-\pi-\tau$ spin echo sequence was τ = 50 µs. Averaging of 50.000 spin echoes or more was performed [11, 14]. The ^{195}Pt SEHS NMR spectra in **Fig. 6** were acquired using an B_0 = 8 T Oxford magnet and point-by-point by a frequency-swept spin echo technique ($\pi/2-\tau-\pi-\tau$) between ν_0 = 69.5 and 74.0 MHz. The delay between the $\pi/2$ and the π pulses was τ = 35 µs, while the pulse lengths were 5 and 10 µs, respectively [11]. The ^{195}Pt chemical shifts were referenced to a 1.2 M solution of Na_2PtCl_6 in D_2O [29]. The SEDOR experiments leading to the spectrum in **Fig. 8** were performed with pulse lengths 2.2 and 4.8 µs for the $\pi/2$ and π pulses, respectively, applied to the ^{195}Pt nuclei, and a π pulse of 44 µs applied to the ^{13}C nuclei. The spectra were recorded with the samples immersed in liquid nitrogen, i.e. at T = 77 K [33].

References:

[1] S. Mandal, D. Roy, R.V. Chaudhari, M. Sastry, *Pt and Pd nanoparticles immobilized on amine-functionalized zeolite: Excellent catalysts for hydrogenation and Heck reactions*, Chem. Mater. 16 (2004) 3714-3724, DOI: 10.1021/cm0352504.

[2] U. Obenaus, F. Neher, M. Scheibe, M. Dyballa, S. Lang, M. Hunger, *Relationships between the hydrogenation and dehydrogenation properties of Rh-, Ir-, Pd-, and Pt-containing zeolites Y studied by in situ MAS NMR spectroscopy and conventional heterogeneous catalysis*, J. Phys. Chem. C 120 (2016) 2284-2291, DOI: 10.1021/acs.jpcc.5b11367.

[3] J. Weitkamp, *Catalytic hydrocracking – Mechanisms and versatility of the process*, ChemCatChem 4 (2012) 292-306, DOI: 10.1002/cctc.201100315.

[4] A. Corma, A. Martinez, S. Pergher, S. Peratello, C. Perego, G. Bellusi, *Hydrocracking-hydroisomerization of n-decane on amorphous silica-alumina with uniform pore diameter*, Applied Catalysis A: General 152 (1997) 107-125, DOI: 10.1016/S0926-860X(96)00338-9.

[5] H. Lee, H. Kim, M.J. Yu, C.H. Ko, J.-K. Jeon, J. Jae, S.H. Park, S.-C. Jung, Y.-K. Park, *Catalytic hydrodeoxygenation of bio-oil model compounds over Pt/HY catalyst*, Scientific Reports 6 (2016) 28765, DOI: 10.1038/srep28765.

[6] S. Rabl, D. Santi, A. Haas, M. Ferrari, V. Calemma, G. Bellussi, J. Weitkamp, *Catalytic ring opening of decalin on Ir- and Pt-containing zeolite Y – Influence of the nature of the charge-compensating alkali cations*, Microporous Mesoporous Mater. 146 (2011) 190-200, DOI: 10.1016/j.micromeso.2011.03.045.

[7] A. Haas, S. Rabl, M. Ferrari, V. Calemma, J. Weitkamp, *Ring opening of decalin via hydrogenolysis on Ir/- and Pt/silica catalysts*, Appl. Catal. A: General 425-426 (2012) 97-109, DOI: 10.1016/j.apcata.2012.03.010.

[8] G.J. Rees, S.T. Orr, L.O. Barrett, J.M. Fisher, J. Houghton, G.H. Spikes, B.R.C. Theobald, D. Thompsett, M.E. Smith, J.V. Hanna, *Characterisation of platinum-based fuel cell catalyst materials using ^{195}Pt wideline solid state NMR*, Phys. Chem. Chem. Phys. 15 (2013) 17195-17207, DOI: 10.1039/c3cp52268g.

[9] U. Obenaus, S. Lang, R. Himmelmann, M. Hunger*, In situ MAS NMR investigation of parahydrogen induced hyperpolarization inside meso- and micropores of Ir-, Pt-, Rh-, and Pd-containing solid catalysts*, J. Phys. Chem. C 121 (2017) 9953-9962, DOI: 10.1021/acs.jpcc.7b01899.

[10] J.P. Bucher, J. Buttet, J.J. van der Klink, M. Graetzel, E. Newson, T.B. Truong, *^{195}Pt NMR studies of supported catalysts*, Colloids Surf. 36 (1989) 155-167, DOI: 10.1016/0166-6622(89)80234-3.

[11] J. P. Bucher, J.J. van der Klink, *Electronic properties of small supported Pt particles: NMR study of ^{195}Pt hyperfine parameters*, Phys. Rev. B 38 (1988) 11038-11047, DOI: 10.1103/PhysRevB.38.11038.

[12] C.P. Slichter, *NMR study of platinum catalysts*, Surf. Sci. 106 (1981) 382-396, DOI: 10.1016/0039-6028(81)90226-0.

[13] J.P. Bucher, J. Buttet, J.J. van der Klink, *Electronic properties and local densities of states in clean and hydrogen covered Pt particles*, Surf.Sci. 214 (1989) 347-357, DOI: 10.1016/0039-6028(89)90175-1.

[14] H.E. Rhodes, P.-K. Wang, H.T. Stokes, C.P. Slichter, *NMR of platinum catalysts. I. Line shapes*, Phys. Rev. B 26 (1982) 3559-3568, DOI: 10.1103/PhysRevB.26.3559.

[15] Y.Y. Tong, J.J. van der Klink, G. Clugnet, A.J. Renouprez, D. Laub, P.A. Buffat, *Electron microscopy and ^{195}Pt nuclear magnetic resonance of platinum particles in a zeolite-Y matrix*, Surf. Sci. 292 (1993) 276-288, DOI: 10.1016/0039-6028(93)90333-F.

[16] Y.Y. Tong, J. J. van der Klink, *Hydrogen adsorption on platinum particles studied by ^{195}Pt NMR,* J. Phys. Chem. 98 (1994) 11011-11014, DOI: 10.1021/j100094a005.

[17] Y.Y. Tong, J.J. van der Klink, *Local metal to non-metal transition on oxygen-covered platinum particles from ^{195}Pt nuclear magnetic resonance*, J. Phys.: Condens. Matter 7 (1995) 2447-2459, DOI: 10.1088/0953-8984/7/12/009.

[18] Y.Y. Tong, D. Laub, G. Schulz-Ekloff, A.J. Renouprez, J.J. van der Klink, *Indications from ^{195}Pt NMR for a temperature-dependent metal-nonmetal transition of small platinum particles in zeolites*, Phys. Rev. B 52 (1995) 8407-8413, DOI: 10.1103/PhysRevB.52.8407.

[19] W.G. Clark, M.E. Hanson, F. Lefloch, P. Segransan, *Magnetic resonance spectral reconstruction using frequency-shifted and summed Fourier transform processing*, Rev. Sci. Instrum. 66 (1995) 2453-2464, DOI: 10.1063/1.1145643.

[20] I.J.F. Poplett, M. E. Smith, *Field sweep broadline NMR spectroscopy*, Solid State Nucl. Magn. Reson. 11 (1998) 211-214, DOI: 10.1016/S0926-2040(97)00110-0.

[21] E. Roduner, Ch. Jensen, J. van Slageren, R. A. Rakozy, O. Larlus, M. Hunger, *Anomalous diamagnetic susceptibility in 13-atom Pt nanocluster superatoms*, Angew. Chem. Int. Ed. 53 (2014) 4318-4321, DOI: 10.1002/anie.201310637.

[22] S. Ino, *Stability of multiply-twinned particles*, J. Phys. Soc. Jpn. 27(4) (1969) 941-953, DOI: 10.1143/JPSJ.27.941.

[23] S.J. Tauster, S.C. Fung, R.L. Garten, *Strong metal-support interactions. Group 8 noble metals supported on titanium dioxide*, J. Am. Chem. Soc. 100 (1978) 170-175, DOI: 10.1021/ja00469a029.

[24] Y.Y. Tong, C. Rice, N. Godbout, A. Wieckowski, E. Oldfield, *Correlation between the Knight shift of chemisorbed CO and the Fermi level local density of states at clean platinum catalyst surfaces*, J. Am. Chem. Soc. 121 (1999) 2996-3003, DOI: 10.1021/ja9830492.

[25] Y.Y. Tong, C. Rice, A. Wieckowski, E. Oldfield , *^{195}Pt NMR of platinum electrocatalysts: Friedel-Heine invariance and correlations between platinum Knight shifts, healing length, and adsorbate electronegativity*, J. Am. Chem. Soc. 122 (2000) 11921-11924, DOI: 10.1021/ja002254q.

[26] T. Fujii, K. Iwamoto, Y. Nakai, T. Shiratsu, H. Yao, K. Ueda, T. Mito, *NMR evidence for energy gap opening in thiol-capped platinum nanoparticles*, Phys. Rev. B 105 (2022) L121401, DOI: 10.1103/PhysRevB.105.L121401.

[27] L.E. Marbella, J.E. Millstone, *NMR techniques for noble metal nanoparticles*, Chem. Mater. 27 (2015) 2721-2739, DOI: 10.1021/cm504809c.

[28] J. Korringa, *Nuclear magnetic relaxation and resonance line shift in metals*, Physica 16 (1950) 601-610, DOI: 10.1016/0031-8914(50)90105-4.

[29] R.K. Harris, E.D. Becker, S.M. Cabral de Menezes, R. Goodfellow, P. Granger, *NMR nomenclature: Nuclear spin properties and conventions for chemical shifts, IUPAC recommendations 2001*, Solid State Nucl. Magn. Reson. 22 (2002) 458-483, DOI: 10.1006/snmr.2002.0063.

[30] J.S. Buchanan, G.A. Hards, S.J. Copper, GB Pat., 2,242,203, 1991.

[31] F. Wen, H. Bonnemann, R. J. Mynott, B. Spliethoff, C. Weidenthaler, N. Palina, S. Zinoveva, H. Modrow, *Preparation of Pt_{13} clusters in the presence of trialkylaluminium* , Appl. Organomet. Chem. 19 (2005) 827-829, DOI: 10.1002/aoc.913.

[32] J.P. Bucher, J. Buttet, J.J. van der Klink, M. Graetzel, E. Newson, T.B. Truong, *Preparation, characterization and NMR spectra of platinum on alumina catalysts in relation to their activity and stability*, J. Mol. Catal. 43 (1987) 213-220, DOI: 10.1016/0304-5102(87)87008-6.

[33] C.D. Makowka, C.P. Slichter, J.H. Sinfelt, *NMR of platinum catalysts: Double NMR of chemisorbed carbon monoxide and a model for the platinum NMR line shape*, Phys. Rev. B 31(9) (1985) 5663-5679, DOI: 10.1103/PhysRevB.31.5663.

[34] E.R.H. van Eck, W.S. Veeman, *The determination of the average ^{27}Al -^{31}P distance in aluminophosphate molecular sieves with SEDOR NMR*, Solid State Nucl. Magn. Reson. 1 (1992) 1-4, DOI: 10.1016/0926-2040(92)90003-R.

[35] C. Brown, B.T. Heaton, P. Chini, A. Fumagalli, G. Lorigini, *Stereochemical non-rigidity of a metal polyhedron: Fourier transform platinum-195 nuclear magnetic resonance spectra of $[Pt_n(CO)_{2n}]^{2-}$(n = 3, 6, or 9),* J. Chem. Soc. Chem. Commun. (1977) 309-311, DOI: 10.1039/C39770000309.